1-17-2015

Statistical Variation of Diverse Light Emission Measurements from Bisphenol/Amine Epoxy Under Energetic Electron Bombardment

Justin Christensen
Utah State University

Recommended Citation

Department of Physics 4900 Project Research Mentor: J.R. Dennison January 17, 2015

Statistical Variation of Diverse Light Emission Measurements from Bisphenol/Amine Epoxy Under Energetic Electron Bombardment

Justin Christensen

Department of Physics
4900 Project
Research Mentor: J.R. Dennison
January 17, 2015

Abstract:

Dielectric materials subjected to energetic electron fluxes can emit light in several forms. We have observed three distinct types of emissions: (i) short-duration (<1 ms), high-intensity electrostatic discharge (ESD) or "arc" events; (ii) intermediate-duration, high-intensity events which begin with a bright arc followed by an exponential decay of intensity (~10 to 100 s decay constant), termed "flares"; and (iii) long-duration, low-intensity emission, or cathodoluminescence, that continues as long as the electron flux is on. These events were studied for bulk samples of bisphenol/amine epoxy, using an electron gun with varying current densities (0.3 to 5 nA/cm^2) and energies (12 to 40 keV) in a high vacuum chamber. Light emitted from the samples was measured with a high-sensitivity visible to near-infrared video camera. Results of the spatial and temporal extent for each type of event are presented as well as a discussion of how absolute spectral radiance and rates for each type of event are dependent on incident electron current density, energy, and power density and on material type, temperature, and thickness. Applications of this research to spacecraft charging and light emissions are discussed.

Motivation:

Spacecraft materials can glow when bombarded by energetic electrons in the space-plasma environment.[1] Photon emission caused by energetic electrons is called "cathodoluminescence". In space-based observatories this can cause detectors to be exposed to light that did not originate at the objects being observed. It is crucial to understand how the emissions from various spacecraft materials compare in intensity and spectral range to natural sources of light contamination for space-based observatories to maximize their sensitivity.

Spacecraft charging is also a very large concern due to the potential for damage to sensitive electronic circuits.[2] The dynamic interplay between the space-plasma environment and spacecraft materials involves electron interaction with material surfaces (i.e., electron yield),[3] charge deposition range, and electron transport in the material (conductivity). Each of these interactions can affect one another and creates a very complex problem when the system is not in equilibrium; however the link between cathodoluminescence and each of these gives us a tool which can help in our endeavor to understand these processes.[4]

Background:

There are three distinct forms of photon emission which have been observed in this type of environment (Fig. 1).

Cathodoluminescence, termed "glow", is the continuous emission of photons when energetic electrons are incident upon a disordered insulating material. Collisions between electrons and molecules in the material lattice excite valence electrons into the conduction band. These excited electrons quickly decay into short-lived, shallow trap states, until they finally fall down to deeper more permanent trap states (release photons).[5] Therefore cathodoluminescent intensity varies with the rate at which electrons are being excited (has to do with incident electron flux, and energy), the density of electron trap states (material property), and the number of open lower-level traps (charge dissipation).

Jensen *et al.*[5] have developed a model which relates the cathodoluminescent intensity to incident electron properties and other material properties.

$$I_\gamma(J_b, E_b, T)\alpha \frac{D(J_b,E_b)}{D+D_{sat}}(1 - e^{\varepsilon_{ST}/k_bT}) \quad (1)$$

$$D(J_b, E_b) = \frac{E_b J_b(1-\eta(E_b))}{q_e \rho_m} \times \begin{matrix} 1/L & if\ R(E_b)<L \\ 1/R(E_b) & if\ R(E_b)>L \end{matrix}$$

where

I_γ = Luminescent Intensity
J_b = incident current density
E_b = incident beam energy
T = temperature
D = dose rate
R = range
D_{sat} = saturation dose rate
q_e = electron charge
ρ_m = material density
η = back scattered electron yield
ε_{ST} = ΔE from shallow traps to conduction band

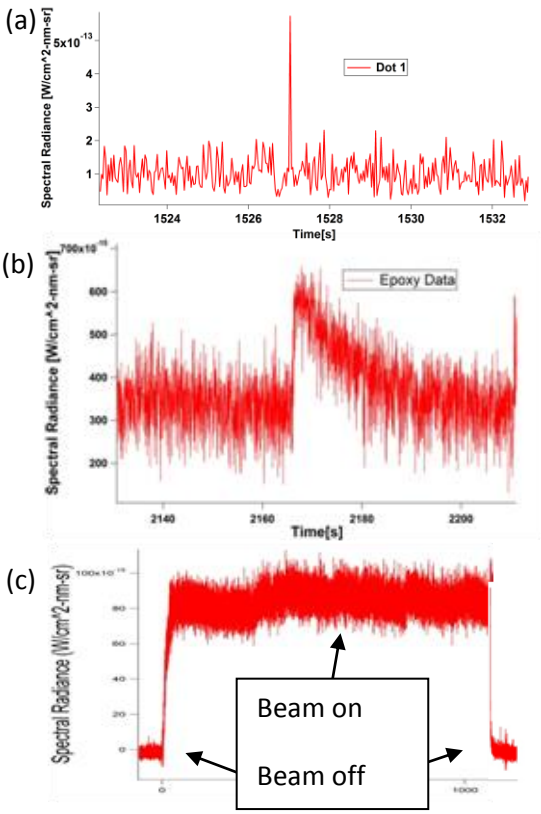

Fig. 1 Electron-induced photon emission. (a) arcs generally appear in one frame because they are so short. (b) Flares appear as an initial bright spike with an exponential decay with a 40 s decay time. (c) Glow is the constant emission of light whenever the beam is on.

Arcs are very short duration (<1ms) flashes caused by rapid discharge from a charged body which can cause electrostatic breakdown of the material. They are assumed to be random events which occur when built up charge produces an electric field large enough for electrostatic breakdown to occur. This causes damage to the material and produces intense photon emissions.

Flares are intermediate duration photon emissions which begin with a bright arc and are followed with an exponential decay of intensity (10 to 100 s. exponential decay constant). Flares may be sudden discharges of the material related to radiation induced conductivity, RIC, when very energetic cosmic rays pass through material.[6]

All three types of photoemission were examined for bisphenol/amine epoxy as the incident electron fluxes and energies were varied. This type of study has been done previously for individual samples of bisphenol/amine epoxy.[7] The main point of this study was to analyze several samples (36 "glue dots" Fig. 2) of this epoxy exposed simultaneously to nearly identical electron fluxes to better understand stochastic variations.

Procedures:

The data for this project were collected by Justin Dekany (USU), Chuck Bowers (GSFC), and Todd Schneider (MSFC) at Marshall Space Flight Center. The epoxy "glue dot" samples were mounted inside a vacuum chamber on a Black Kapton

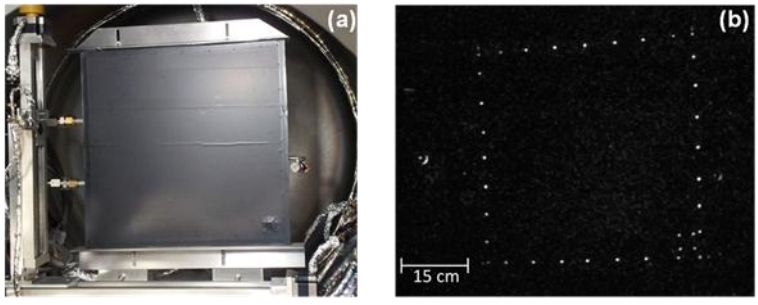

Fig. 2: (a) 41x41 cm sample mounted in MSFC vacuum chamber. (b) 36 "glue dots" luminescing around the periphery of the other sample.

substrate which was cooled to the boiling point of liquid nitrogen. (Fig. 3) An electron gun was used to bombard the sample with electrons of a known energy and flux density (similar to what would be seen in a typical space environment). On the back of the sample was a large metal plate which was connected to a picoammeter used to measure the incident electron current density throughout the tests. Photon emission was monitored with a high sensitivity black and white CCD camera sensitive to wavelengths of about 650 ± 250 nm.

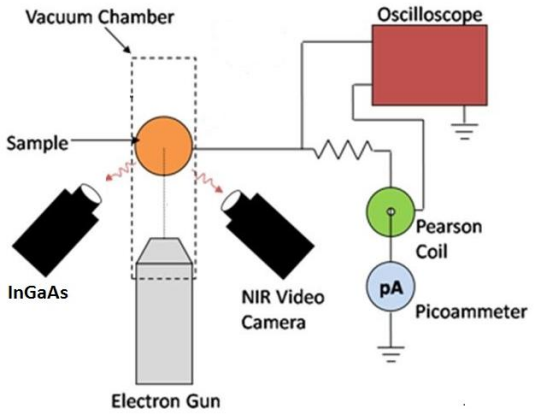

Fig. 3: Rough schematic showing the experimental setup with sensors and other apparatus.

In order to analyze the data later it was important that the electrometer files, and video files could be synchronized. To do this, a timing-light was turned on, and then as the electron beam was turned on the light was turned off. This made it possible to find simultaneous events in electrometer and video data.

Data Analysis:

CCD cameras use an array of photosensitive cells to measure the number of incident photons across the image plane of the camera. The number of photons incident on each bin is converted to a bit value between zero and some maximum bit value. The camera used is calibrated using a NIST traceable light source which has a known radiance over a range of wavelengths.[8] The camera is further calibrated using neutral density filters to give information for varying intensities. The pixel response is linear with the incident intensity which gives a calibration factor to convert from pixel values to absolute spectral radiance. The calibration factor for the setup used was determined to be $\mathrm{CF} = 3.359 * 10^{-15}\ \frac{\mathrm{W}}{\mathrm{cm^2 nm * sr}} / \frac{\mathrm{Counts}}{\mathrm{Pixel}}$.

To analyze the video data each file is stripped in to individual .jpg images. These JPEG images are analyzed by a MatLab® program, designed for this project, which allows the user to select multiple regions of the image for analysis. It sums the pixel values in each sample region for every frame and then creates an output file which contains these sums as well as the number of pixels in each area. Analysis of sequential frames creates an array of calibrated intensities versus time for each region.

An Igor-pro® routine has been developed which takes the output data from the MatLab® program as well as the electrometer data collected, removes stray light contamination from the video data, and converts it to photon intensity (absolute spectral radiance). To remove stray light the average pixel value is measured for each region when the e^- beam is blanked. This gives the appropriate light contamination due to the electron gun filament for each frame region, which is subtracted from the data to zero it. The adjusted pixel total is then divided by the number of pixels in each area which gives an average pixel value, and multiplication by the calibration factor converts the average pixel value to average absolute spectral radiance [2] In terms of program variables.

$$ASR = \left(\frac{T_s - Ave_{Off}}{N_s}\right) * CF \qquad [2]$$

where

ASR = Absolute spectral radiance
N_s = Number of pixels in the area
T_s = Sum of pixel values in sample area
Ave_{Off} = Average Total of pixel values in sample area when beam is blanked
CF = Calibration factor

Statistical analysis is done for steady intensity segments of each run for every sample. These data are then combined by averaging to reduce the error. These data are plotted versus the incident electron power density, which is calculated by multiplying the electron energy and current flux density to give $\mu W/cm^2$.

Flare Rate:

To determine the flare rate for a certain beam setting, smoothed intensity graphs are made for each epoxy dot, in order to eliminate noise and display flares more visibly (Fig. 4). The number of flares is then counted for each dot at a given beam setting and divided by the amount of time that the beam was on that setting to determine the flare rate (3):

$$\frac{Flares}{sec} = \frac{N_f}{t_{beam}} \qquad (3)$$

N_f = number of flares.
t_{beam} = beam-on time length.

Arc Rate:

The determination of the arc rate is a much trickier. The reason for this is that arcs have varying radiant intensities and last for very small time intervals. This means that although the brightest arcs stand out, the fainter arcs cannot be distinguished from the noise. Also the experimental procedure used caused the noise envelope to be much larger than what is usually seen during measurements conducted at USU. A systematic method was desired to determine a threshold at which arcs could be defined by. The methods used involved the following:

(i) Determination of the average and standard deviation of the intensity to establish the inherent noise level using the average plus a multiple of the standard deviation as a threshold
(ii) Determine the average and minimum of the intensity data, take their difference, and use the average plus some multiple of the difference as a threshold

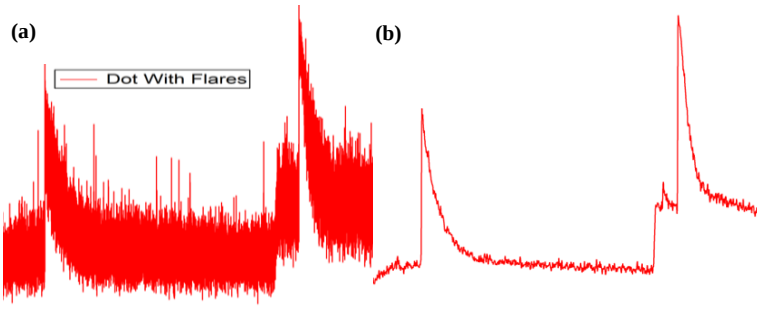

Fig. 4) Two graphs of the same data. (a) Unsmoothed data, 2 flares visible, lots of noise. (b) Smoothed data flares are clearly visible; A small flare is visible due to noise reduction.

(iii)Make a histogram of the intensity data and use the right edge of the distribution as a threshold.

Arc Correlation:

The method for determining arc correlation in neighboring samples involved the following :

(i) Consider every arc in the i^{th} "glue dot".
(ii) If another arc occurs within 0.03 sec (one video frame) afterwards in the j^{th} "glue dot", it is counted as a correlated arc.
(iii) Correlation values are calculated as the ratio of correlated arcs in the j^{th} sample to total arcs in the i^{th} sample.
(iv) This value is equal to 1 for self-correlation i=j.
(v) Values between 0 and 1 are seen for different samples with larger values for higher correlations.

$$correlation\ value = C_{(i,j)} \equiv N_{(i,j)} \ / \ N_{total(i)} \qquad [4]$$

where

$$N_{(i,j)} \equiv arcs\ in\ j\ correlated\ to\ an\ arc\ in\ i$$
$$N_{total(i)} \equiv number\ of\ arcs\ in\ i$$

Results:

Glow:

Figure (4) compares this analysis of multiple regions to previous analyses done for the "glue dots". The black data points show the results from an edge region which contained the epoxy dots as well as Black Kapton. Due to the fact that the cathodoluminescent intensity of the epoxy is much brighter than Black Kapton, and the Black Kapton took up about 50 X more area than the epoxy, this lowered the measured glow. The red data show the analysis for one single epoxy dot which gives more accurate results for the glow. The uncertainty is much larger because there are fewer pixel points to do statistical analysis on. The green/blue data are the data which were analyzed in this experiment. The green curves are data taken immediately after fluctuations in the electron beam occurred. This produced a linear

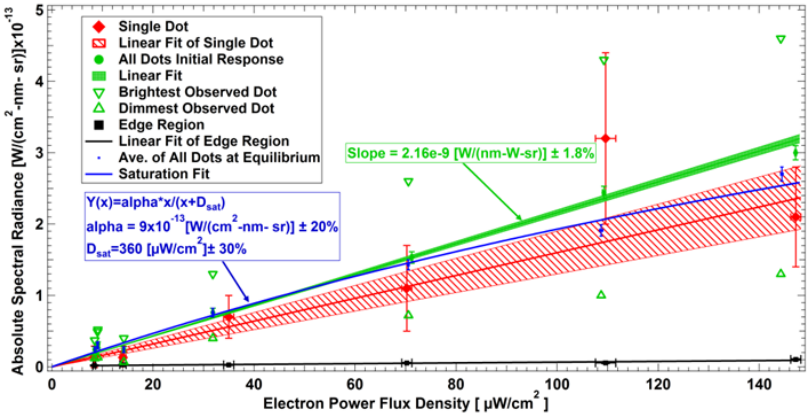

Fig. (4). Comparison of this multi-region analysis (green and blue) to previous analyses (red and black).

correlation between the electron power density and the glow it produced. The blue data were taken from steady sections of the run after the system had time to come to equilibrium. This produced a saturation effect at higher electron dose rates. The uncertainty for these data was ≈ 6 times smaller than the red data because there were 36 times more data points for statistical analysis.

Flare Rate:

It was found for this analysis that some of the epoxy dots were more active than others. For example 10 of the epoxy samples had 2 to 4 flares during the 26 minute 25 keV run, while 13 of the 36 samples had none. Possible reasons for the variation in activity are: variations of shape which could affect peak electric fields, presence of contaminants, air bubbles, variations in the electron beam profile, and stochastic nature of flares. Figure 5 shows the results for this analysis and previous analyses. The blue data in this graph are from the edge region analysis. Because there were 36 dots in this region there should be 36 times more flares observed than the single dot, and average of the 36 dots. This was not seen experimentally; therefore, the method used to analyze the edge region was likely not as accurate. This may have been because of the large area of the edge region. This would make fluctuations due to flares smaller making it harder to distinguish them from the glow or background contamination. The black and red data are the single dot and 36 averaged dots, respectively. The single dot analyzed here was chosen because it appeared to be a more active dot (used to give worst case data results). The analysis done for this experiment gave a nice linear fit for the data above a threshold electron power density of ≈ 30 μW/cm^2 (± 40 %) with a flare rate of (0.07 ± 0.01) (flares/hr)/ (μW/cm^2)

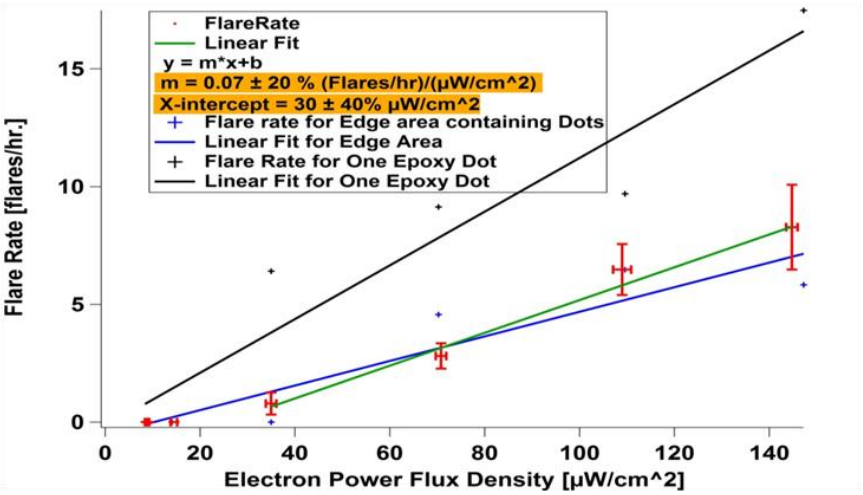

(Fig. 5) Comparison of flare analysis to previous analyses done on "glue dots".

Comparison of Flare/Arc Spatial Extent:

The images in Fig. 6 show the same region from various video frames superimposed on each other to compare the spatial extent of flares and arcs. The superimposed arcs were colored blue to differentiate them from the flare in the background. As can be seen flares tend to light up most, if not all, of the sample area, whereas arcs appear to be small,

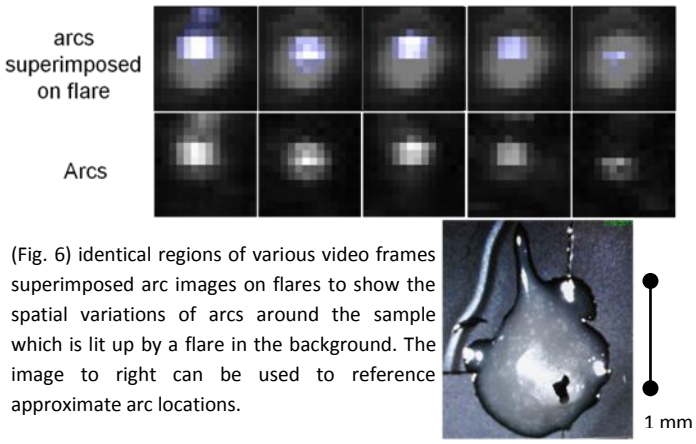

(Fig. 6) identical regions of various video frames superimposed arc images on flares to show the spatial variations of arcs around the sample which is lit up by a flare in the background. The image to right can be used to reference approximate arc locations.

localized, and randomly located events. For this particular sample most of the arcs were in the top left region of the sample, which is of interest because of the asperity which can be seen in the microscope image of the sample (shown below the arc frame in Fig. 6) because fields can be expected to be stronger at the asperity.

Arc Rate:

Although several algorithms were used to identify arcs, they all gave the same unexpected and counterintuitive result of lower arc rates for higher electron power densities. The arc rate data in Fig.7 were obtained using the average intensity minus the minimum intensity as the arc threshold value. Vertical error bars were calculated using the standard deviation of all 36 dot arc rates, and horizontal error bars were calculated using fluctuations in electrometer data. The fit used is an exponential decay of arc rate with increasing power density with a decay constant of 53 μW/cm^2 (±10%). The rate reduction at higher dose rates may be caused by enhanced radiation induced conductivity (RIC) at the higher fluxes. More flares, and more unsaturated charging regions, occur at higher incident power levels; however, increased leakage current from these regions due to enhanced RIC may extend the time required to charge these regions to sufficient magnitude to initiate an arc. Alternately, the higher fluxes may produce additional defects at a higher rate, causing a similar increased conductivity and extended charging time; however, the total incident doses in these experiments seem too low to produce significant numbers of new defects.

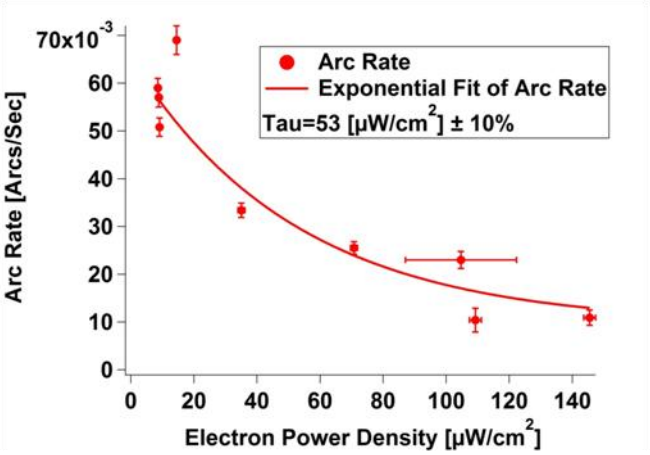

Fig 7) Arc Rate vs Electron Power Density graph showing unexpected result of lower arc rates at higher dose rates.

Stimulated Arc Correlation:

The possibility that a given arc might stimulate arcs in adjacent "glue dots" was investigated through correlation analysis. The dependence of such correlations with "glue dot" separation was also tested. To compare the correlation values described above spatial locations were determined for each "glue dot". The distance between glue dots was then calculated using the Pythagorean theorem. Coincidence was defined by arcs which occurred within ± 1 frame of each other. The correlation values were then graphed versus the distance between samples to look for relations between nearby "glue dots". For low energies little to no correlation was observed; however, at 40 keV some correlation was observed (Fig 8). The

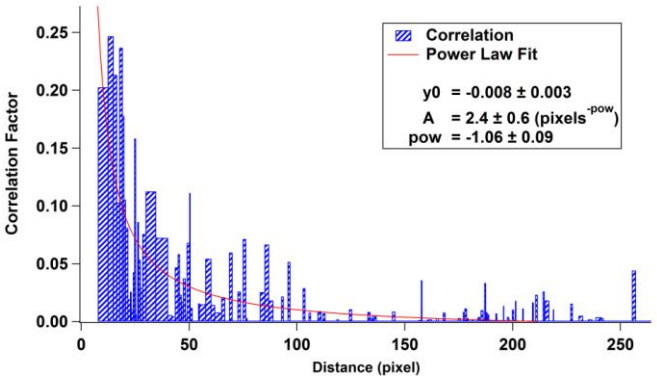

Fig 8) Arc correlation vs. separation for the 40 keV run. A power law fit is shown with a power of ~-1 which is consistent with the r $^{-1}$ fall off of current flux density spreading out on a 2D substrate.

thought behind this is that at higher energies more samples are charged close to the breakdown field at any given time. A discharge in one "glue dot" may cause a sudden spike in the electric field of neighboring "glue dots" which could trigger premature arcing. Such stimulated arc rates might reasonably be expected to scale with electric field intensity. If confined to a 2D surface the field would fall off as r^{-1} where r is the separation distance. The fit to the data in Fig. 8 is a power law with a power of -1.06 ± 0.09, which is consistent with a 1/r fall off of field strength for charges spreading out across a 2D conducting surface.

Conclusion:

The statistical analysis of a larger sample set (36 x larger) reduced uncertainties of glow intensity and arc and flare rates by a factor of ≈ 6. Analysis of many small samples allowed for features like saturation, and flares to be observed more easily. Initial (unsaturated) glow intensity is linear with incident electron power. Equilibrium glow intensity shows hyperbolic dependence on incident electron power, consistent with saturation theory. Flare intensity exponential decrease has similar time constants as initial glow intensity decrease when the beam is turned on and glow intensity increase after decreasing incident power density. Arcs appear as localized phenomena whereas glow and flares are evident over full epoxy dot surfaces. Arcs appear to be mostly random events with some spatial correlation at higher energies between adjacent dots that falls off inversely with dot separation.

For bisphenol/amine epoxy, the higher precision best estimates for material properties are:

- Spectral radiance per incident power density = $(1.98 \pm 0.04)\times10^{-9}$ [W/cm^2-nm-sr per μW/cm^2]
- Saturation dose rate = [420 μW/cm^2] (± 30%)
- Saturation / De-saturation time constants =120 ± 40 [s]
- Flare decay constant = 80 ± 30 [s]
- Flare rate per incident power density = (0.07 ± 0.01 [(Flares/hr)/(μW/cm^2)])
- Threshold electron power density for flares = 30 μW/cm^2 (±40%)
- Arc rate = 1-3 [Arcs/min] (decreasing exponentially with increase of incident energy)

Future work:

A deeper analysis of photon intensity distributions would be useful to aid in understanding just how much light at different intensities is being given off. It would also be better to isolate the current coming from individual epoxy dots so that better information about charge dissipation for each dot could be acquired (potentially allowing us to see arcs in electrometer data). Alternately, surface voltage measurements for each dot could provide similar information.

When CCD's have regions where more electrons are excited than can be accommodated within the potential well excess electrons can spill over into neighboring wells (called "blooming"). A better understanding of this phenomenon could potentially allow us to extract

intensity data from saturated regions of data by calculating how many electrons bled out into neighboring pixels around the sample region.

The science involved in this experiment has many possibilities for further research. One idea that would be of interest is using the spectral "fingerprint" given off by satellites to catalog all the satellites orbiting our planet and to monitor those which pose a potential threat.[1] This could allow the acquisition information about what materials are in use on these satellites, and in what concentrations.

References

[1] Dale C. Ferguson, Jeremy-Murray Krezan, David A. Barton JR Dennison, and Stephen Gregory, "On the Feasibility of Detecting Spacecraft Charging and Arcing by Remote Sensing," Paper Number, AIAA-2013-2828, 5th AIAA Atmospheric and Space Environments Conference, San Diego, CA (2013)

[2] D. Hastings, H. Garrett, Spacecraft-Environment Interactions, New York, NY: Cambridge Press, 1996.

[3] Hoffmann, R., J. Dennison, et al. (2008). "Low-Fluence Electron Yields of Highly Insulating Materials." IEEE Transactions on Plasma Science 36(5 Part 2): 2238-2245.

[4] JR Dennison, Justin Dekany, Jodie Corbridge Gillespie, Phil Lundgreen, Allen Andersen, Amberly Evans Jensen, Gregory Wilson, Alec M. Sim, and Ryan Hoffmann, "Synergistic Models of Electron Emission and Transport Measurements of Disordered SiO2," Invited Seminar, *13th Spacecraft Charging Technology Conference*, (Pasadena, CA, June 25-29, 2014).

[5] Amberly Evans Jensen, "Space Plasma Environment Induced Luminescence of Materials on Space Based Observatories," MS Thesis, 2014.

[6] Kenneth Zia, Justin Dekany and JR Dennison, "Cathodoluminescence Events Coincident with Muon Detection," *American Physical Society Four Corner Section Meeting*, Utah Valley University, Orem, UT, October 17-18, 2014.

[7] Justin Dekany, Justin Christensen, JR Dennison, Amberly Evans Jensen, Gregory Wilson, Todd Schneider, Charles W. Bowers and Robert Meloy, "Variations in Cathodoluminescent Intensity of Spacecraft Materials Exposed to Energetic Electron Bombardment," Abstract 179, *Proceedings of the 13th Spacecraft Charging Technology Conference*, (Pasadena, CA, June 25-29, 2014), 7 pp.

[8] Justin Dekany, Robert H. Johnson, Gregory Wilson, Amberly Evans and JR Dennison, "Ultrahigh Vacuum Cryostat System for Extended Low Temperature Space Environment Testing," *IEEE Trans. on Plasma Sci*., 42(1), 2014, 266-271

[9] Justin Dekany, Justin Christensen, JR Dennison, Amberly Evans Jensen, Gregory Wilson, Todd Schneider, Charles W. Bowers and Robert Meloy, "Variations in Cathodoluminescent Intensity of Spacecraft Materials Exposed to Energetic Electron Bombardment," submitted to *IEEE Tran. Plasma Science*, 2014, 7 pp.